Polymer Testing 35 (2014) 34–44

Contents lists available at ScienceDirect

Polymer Testing

journal homepage: www.elsevier.com/locate/polytest

Material behaviour

Temperature dependency comparison of ultrasonic wave propagation between injected and sintered thermoplastics

Guillaume Trannoy [a,*], Jean-Pierre Nikolovski [b], Stéphane Holé [c], Didier Périno [d]

[a] ESPCI, Laboratoire de physique et d'étude des matériaux (UMR8213), 10, rue Vauquelin, 75005 Paris, France
[b] CEA, LIST, Sensory and Ambient Interfaces Laboratory, Nano-INNOV, Bât. 861, 91191 Gif sur Yvette, France
[c] UPMC – Sorbonne Universités, Laboratoire de physique et d'étude des matériaux (UMR8213), 10 rue Vauquelin, 75005 Paris, France
[d] HLP Technologies, 390 rue Estienne d'Orves, 92700 Colombes, France

ARTICLE INFO

Article history:
Received 26 November 2013
Accepted 20 February 2014

Keywords:
Ultrasonic velocity measurement
Attenuation measurement
Diffraction effect
Viscous coefficients
Temperature
Relative humidity
ABS
Polyamide

ABSTRACT

Active touch localization based on a learning process of touch-disturbed broadband bending wave propagation in thin objects is used to transform any 3D surface into a multi-touch interface. Fast prototyping permits easy manufacturing of various 3D shapes that can be as quickly transformed into touch interfaces. The drawback is their weak mechanical stability with temperature. This paper details the temperature behavior differences between a sintered plastic such as polyamide polymer of type PA12 and raw injected Acrylonitrile-Butadiene-Styrene composite polymer (ABS), in particular how their physical parameters such as Young's modulus and Poisson's ratio are affected by temperature. Correlatively, longitudinal and transversal waves within injected and sintered plastics are investigated across a commercial temperature range of 10 °C to 70 °C. The internal grain structure in plastics obtained by laser sintering of powder makes these materials prone to stronger damping and clear non-linear temperature dependency of the shear wave velocity compared with injected plastics.

1. Introduction

Human computer interfaces (HCI) can be found in familiar objects of our daily environment. In recent years, touch sensitive shells of any shape have been proposed based on an ultrasonic learning process in which the localization of a touch is derived from the diffraction pattern disturbance of a bending wave generated at various frequencies [1]. A localized touch on a finite object creates a unique disturbance of the acoustic wave that can be recognized to estimate the position of the contact. Usual approaches for estimating the touch position use either shell modes in a permanent regime [2], or transient regime [3]. In any case, the disturbance, which is a combination of viscous absorption and diffraction effects, is very small, of the order of a few percent. For large and thick objects, the touch disturbance may be so small that direct transmission between the emitting and receiving transducers must be avoided [4]. In addition, it drastically depends on the way acoustic waves propagate in the shell. It is known that temperature greatly impacts the mechanical properties of materials, and thus the propagation of acoustic waves. As a consequence, temperature variation has a strong effect on the algorithm recognition efficiency. For instance in [5], two signals taken at different temperatures cannot be reliably correlated because of thermal expansion. Additionally, the effect of temperature variations on a diffuse ultrasonic field is not necessarily linear with temperature, so that the modeling of temperature effect as a linear stretching of the frequency spectrum [6] is incorrect, especially in thermoplastics. Therefore, it is necessary to

* Corresponding author. Tel.: +33 (0) 6 71 19 22 40.
E-mail addresses: guillaume.trannoy@espci.fr (G. Trannoy), jean-pierre.nikolovski@cea.fr (J.-P. Nikolovski), stephane.hole@espci.fr (S. Holé), didier.perino@hlp.fr (D. Périno).

http://dx.doi.org/10.1016/j.polymertesting.2014.02.006
0142-9418/

measure the impact of temperature on viscoelastic properties of these materials.

In this paper, we investigate temperature and humidity dependency of fundamental waves in Acrylonitrile-Butadiene-Styrene polymer (ABS) and sintered polyamide of type "PA12". Such dependency has not been studied previously. ABS is commonly used in industry, whereas PA12 has emerging use in 3D fast prototyping techniques such as Selective Laser Sintering (SLS).

The paper deals first with a description of the experimental set-up in Section 2. Then, in the following two sections, the mathematical treatment to determine transit times of elastic waves through the sample materials is discussed in terms of diffraction and expansion. In Section 5 and Section 6, results on velocity and damping measurements are presented in a temperature range of 10 to 75 °C and for 40 to 80% RH. These results are then discussed and analyzed in the last section before conclusions in order to estimate viscoelastic properties of ABS and PA12.

2. Set-up and protocol

A through transmission technique was used to study the temperature effect on propagation of fundamental waves in two sample materials: injected ABS and sintered PA12. The ABS was bought in plates of different thicknesses. We used a material with commercial name Tecaran manufactured by Ensinger [7] (Nufringen, Germany). Sintered plastics were obtained by SLS in which small powder particles are fused with a laser, layer by layer, to form 3 dimensional objects. In our case, a polyamide PA12 polymer powder was used. The manufacturer 3DSystems [8] (Rock Hill, USA) specifies a mean grain size of 58 μm, with a size dispersion ranging from 25 to 92 μm representing 90% of the particles. Plates of these materials were used and thicknesses were measured using a caliper with accuracy of ±0.01 mm.

The set-up comprises a pair of piezoelectric transducers attached on each side of a plate with a coupling agent (Panametrics SWC – Shear Waves Couplant), as illustrated in Fig. 1(a). A wave is sent through the material from an emitter to a receiver. The sample is placed in a climate chamber KMF240 (Binder, Germany) in order to evaluate thermal coefficients of velocity. Precision is enhanced by using two different thicknesses for each material. Velocities are deduced from transit-time difference over the temperature range. Fundamental waves are excited with a 20 Vpp tone burst of one period sine wave provided by a signal generator, Tektronix AWG3022. Reception is done with a PICOSCOPE ADC212 acquisition board featuring 12 bits of vertical resolution at 50 MSa s^{-1}. All measurements consist of 64 averaged acquisitions and are transferred to a computer and handled in the Matlab environment. Longitudinal and transversal waves are selectively detected using two different Non-Destructive Testing (NDT) transducers from Panametrics (Waltham, Massachusetts). Shear waves are detected at a 1 MHz central frequency with a V153 type, whereas longitudinal waves are detected at a 5 MHz central frequency with the Panametrics M110 type. Transducers face each other and are held tight against the

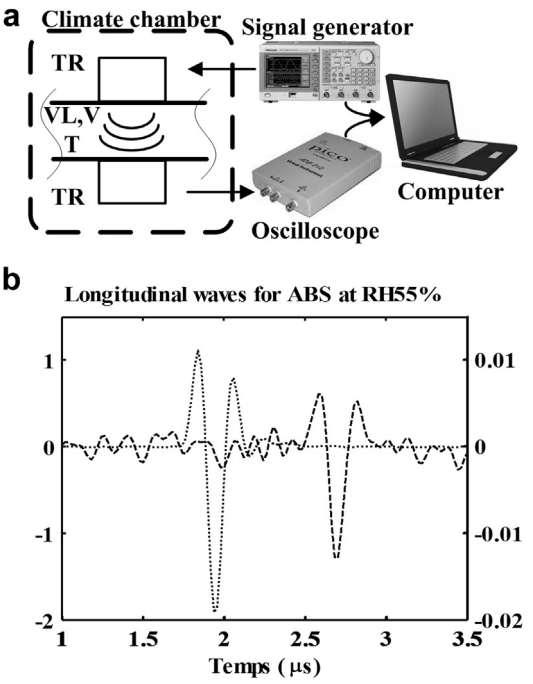

Fig. 1. (a) Set-up with samples conditioned in a climate chamber. Signal generation and data acquisition are controlled in the Matlab environment. (b) Examples of acquired longitudinal waves in ABS (vertical scale in mV). Dotted line: 3 mm thick material. Dashed line: 4.5 mm thick material.

sample by spring loaded clips under a force of ~10 N in order to limit the thickness of the viscous couplant (Panametrics SWC) used both for longitudinal and shear waves. This couplant is sufficiently viscous to transmit transversal waves at temperatures up to 38 °C according to the manufacturer's datasheet. In practice, arrival time can be distinguished at temperatures well above this limit, particularly for longitudinal waves. An example of received signals for two different thicknesses of ABS is illustrated in Fig. 1(b).

Samples are then placed in the climate chamber for controlling the temperature between 10 °C and 75 °C at three different constant Relative Humidity (RH) values of 40%, 55% and 80%. Standard operating condition for a touch interface is RH = 55% whereas RH = 40% and RH = 80% are extreme conditions. Temperatures are logged with a thermocouple coupled to the sample material with thermal paste.

All measurements were repeated on the occasion of various measurement campaigns under the same conditions.

3. Diffraction effect correction

Since the velocity is determined by fine measurement of the transit time, the diffraction phenomenon has to be accounted for. For that purpose, let us express the velocity from the potential of velocity field $\vec{v} = -\vec{\nabla}\,\phi$ and for a monochromatic wave $\phi(R,t) = \phi(R)e^{i\omega t}$, the Rayleigh integral in cylindrical domain defines the potential ϕ:

$$\phi(r,z) = \frac{V_0}{2\pi}\int_0^{2\pi}\int_0^{a}\frac{e^{-ikR}}{R}\cdot\sigma\cdot d\varphi\cdot d\sigma \quad (1)$$

A plane wave of pulsation ω is expressed at distance z as:

$$\phi_{plane}(z) = \frac{V_0}{ik}e^{-ikz} \quad (2)$$

The diffraction correction term is based on the ratio of the diffracted wave by an equivalent plane wave taking into account integration over the same receiver aperture at a distance z from the emitter [9]:

$$D = \frac{\langle\phi(r,z)\rangle_S}{\langle\phi_{plane}(z)\rangle_S} = \left(\frac{ik}{\pi a^2}\right)e^{ikz}\int_0^{2\pi}\int_0^{a}\int_0^{a}\frac{e^{-ikR}}{R}\cdot r\cdot\sigma\cdot dr\cdot d\sigma\cdot d\varphi \quad (3)$$

It is demonstrated in [10] that, if the condition $ka >> 1$ is satisfied, the Fresnel diffraction approximation can be used to obtain the Lommel diffraction correction integral and the diffraction correction term can be expressed using Bessel functions as:

$$D_L(S) = 1 - e^{-i\frac{2\pi}{S}}\left[J_0\left(\frac{2\pi}{S}\right) + iJ_1\left(\frac{2\pi}{S}\right)\right] \text{ with } S = \frac{2\pi z}{ka^2} = \frac{z\lambda}{a^2} \quad (4)$$

The phase of the correction term accounting for diffraction expresses an equivalent additional lag which occurs between a plane and a diffracted wave:

$$t^{diff} = \frac{-\arg(D^{diff})}{\omega}, \quad (5)$$

where $\arg(D^{diff})$ is the phase of the diffraction correction term. Fig. 2 is an example of the calculated pressure field for the M110 longitudinal transducer in ABS at 22 °C. The three vertical lines correspond to the different material thicknesses for the samples (3 mm, 4.5 mm and 10 mm).

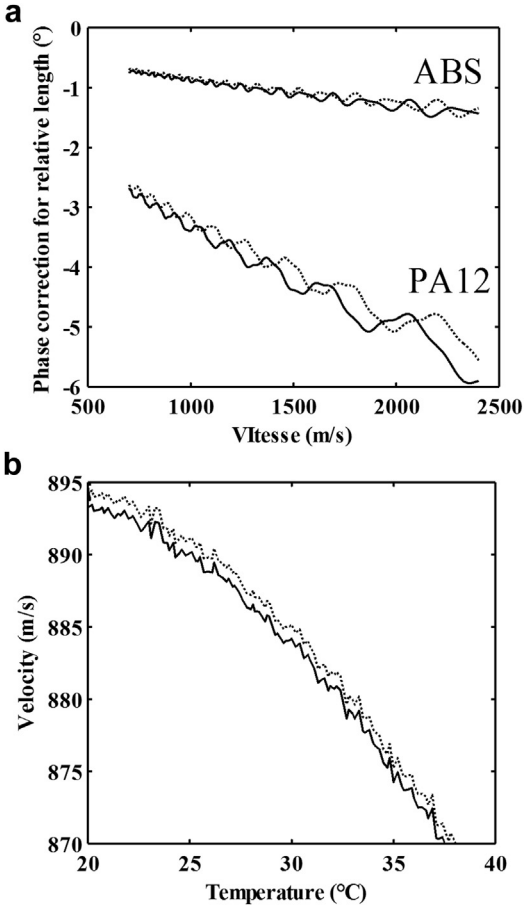

Fig. 3. (a) Phase correction term for relative thicknesses of materials. Top solid Line: ABS with V153 4.5/3 mm. Top dotted Line: ABS with M110 4.5/3 mm. Bottom solid line: PA12 with V153 10/3 mm. Bottom dotted line: PA12 with M110 10/3 mm. (b) Example of correction for transversal velocity in PA12 at 55% RH. Solid line: without correction. Dotted line: with diffraction correction.

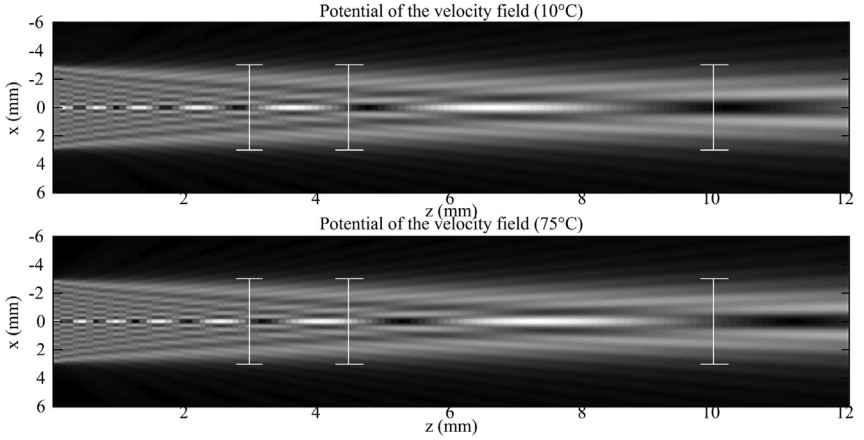

Fig. 2. Diffraction field of potential for Panametrics transducer M110 at 5 MHz central frequency in ABS at a temperature of 10 °C (top), compared with same field at 75 °C (bottom).

In the case of velocity measurements, we do not know a priori the velocity and cannot apply a diffraction correction. The method is then to estimate a rough value of the velocity for a measured propagation delay. This value is then used to calculate a diffraction correction term. After a few iterations the method converges to a stable value of velocity. Fig. 3(a) shows diffraction correction for the two materials and both propagation modes at two relative thickness measurements. We can note the increased value of the correction terms for PA12 associated with a sample of increased thickness from 4.5 to 10 mm. Fig. 3(b) shows a typical graph of velocity versus temperature with and without compensation of the diffraction effect in our measurements. As can be seen, the diffraction effect tends to undervalue the real velocity by 0.13%. Mean errors of velocities due to diffraction are respectively 0.15% and 0.12% for longitudinal and transversal waves in ABS and respectively 0.22% and 0.13% for longitudinal and transversal waves in PA12. Though corrections seem relatively small in that example and generally for velocities, diffraction effect on the attenuations leads to mean error values of, respectively, 2.4% and 3.6% for longitudinal and transversal waves in ABS and, respectively, 6.4% and 2.1% in PA12. The relevance of these errors can be appreciated in regards to the thickness errors which is 0.14% for PA12 and 0.67% for ABS.

4. Dilatation effect correction

The velocity measurement is based on the transit-time measurement in the sample material of a given thickness. However, temperature also has an effect on the sample dimensions which change with dilatation/compression effects. We use the thermal coefficients found in the materials datasheet to calculate a correction factor in the sample thickness due to thermal expansion. For the ABS sample, the manufacturer gives a Coefficient of Thermal Expansion (CTE) of 52 μm m^{-1} K^{-1} (ASTM D696, −30 °C to 30 °C). For the PA12, the CTE given by the manufacturer is 82.6 μm m^{-1} K^{-1} (ASTM E831, 0 °C–50 °C). The maximum variation of differential thickness due to thermal expansion is 0.5% (resp. 0.3%) for PA12 (resp. ABS) over a temperature range of 60 °C.

Consequently, temperature variation affects material density. Densities are given at a temperature of 23 °C as specified by ASTM D792. In these conditions, ABS has a density of 1.04 and PA12 a density of 1. Now, taking into account dilatation effect of a constant mass, density is described by the following law:

$$\rho = \frac{\rho_{23^\circ C}}{\left[1 + C_{ThermExp}(T - 23)\right]^3} \tag{6}$$

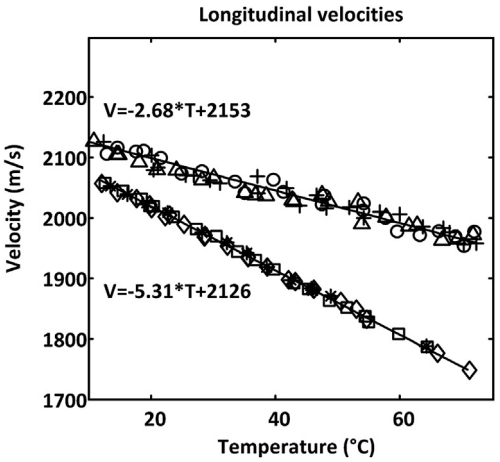

Fig. 4. Longitudinal wave velocities in ABS (+ RH 40%, ○ RH 55%, Δ RH 80%) and sintered plastic of PA12 (◆ RH 40%, □ RH 55%, * RH 80%).

Equation (6) expresses a decrease of density as a result of thermal expansion for ABS and PA12. A density variation of 1.8% (resp. 1%) for PA12 (resp. ABS) is expected in the temperature range of interest. As a consequence, the density has to be taken into account for physical parameter estimation.

5. Velocity measurements

Velocity dependency with temperature is reported under three different RH conditions: 40%, 55% and 80%. These values were chosen in consideration of the climate chamber specifications. At 10 °C the minimum stable RH is 40%. A median value of 55% RH corresponds to standard usage, and the maximum value of 80% RH corresponds to extreme usage conditions of a tactile interface. We measured the differential transit-times between two thicknesses of both sample materials for the entire temperature range, under the three relative humidity conditions and for the two types of waves: longitudinal and transversal. The ABS sample thicknesses were 3.08 mm and 4.66 mm at a temperature of 25 °C. For the PA12, we have 2.92 mm and 10 mm at 25 °C. The propagation delay measurements were made after maintaining the same conditions for 10 hours to ensure homogeneity of temperature and humidity. The measurement started at a temperature of 10 °C and increased to 75 °C at a rate of 0.17 °C min^{-1}. The two types of fundamental waves, longitudinal and transversal at a given RH and for a given material, have a velocity c that can be described for each temperature by the following equation:

$$V(\mathrm{T}, \mathrm{RH}, \mathrm{type}, \mathrm{mat}) = \frac{(h_{high} - h_{low})^* \left[1 + C_{ThermExp}(\mathrm{T} - 25)\right]}{(t_{high} - t_{low}) + t_{tot}^{diff}}, \tag{7}$$

where c is the ratio of the differential thicknesses ($h_{high} - h_{low}$) by the differential transit time ($t_{high} - t_{low}$), $C_{ThermExp}$ is the correction factor due to thermal expansion and $t_{tot}^{diff} = t_{high}^{diff} - t_{low}^{diff}$ is the correction term accounting for the diffraction effect, composed of the correction term of both thicknesses. All of these parameters depend on the type of fundamental wave, RH conditions and considered material. As explained in Section 3, velocities are first evaluated without compensation for the diffraction effect. Then, iterations are carried out to evaluate the diffraction correction term and get new values of velocity until velocity remains stable. Correction of the dilatation effect of the thicknesses is evaluated by estimation of thickness variations with CTE found in datasheets of materials.

A) Longitudinal waves

Fig. 4 reports the measurements of longitudinal velocity of the two materials in the three RH conditions. Measurements are fitted with a linear model for longitudinal velocity in ABS and PA12. The longitudinal velocity of ABS has a coefficient of $\gamma_L = -2.64$ m s^{-1} °C^{-1}, whereas sintered plastic PA12 has a greater coefficient, almost twice as large, of $\gamma_L = -5.31$ m s^{-1} °C^{-1}. ABS velocity presents a value of $V_{L0} = 2153$ m s^{-1} at 0 °C, and $V_{L0} = 2126$ m s^{-1} for PA12. Relative humidity does not affect these values. By comparison, the work of [11] gives a thermal coefficient of -2.5 m s^{-1} °C^{-1} for the longitudinal wave of ABS between -50 °C to $+6$ °C, which is fairly close to our result. Again by comparison, stiffer metallic materials with much higher melting points such as aluminum or copper present smaller thermal longitudinal velocity coefficients of -1.1 m s^{-1} °C^{-1} and -0.5 m s^{-1} °C^{-1}, respectively [12].

B) Transversal waves

Fig. 5 presents measurement results for shear waves in ABS and PA12. ABS exhibits temperature behavior that can be

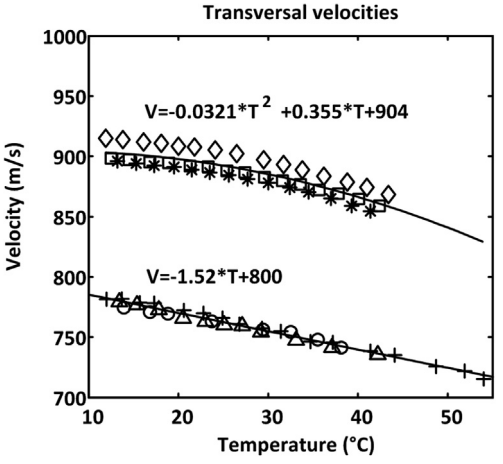

Fig. 5. Transversal wave velocities in ABS (RH 40%, ○ RH 55%, Δ RH 80%) and sintered PA12 (◆ RH 40%, □ RH 55%, * RH 80%). Top curve: PA12. Bottom curve: ABS.

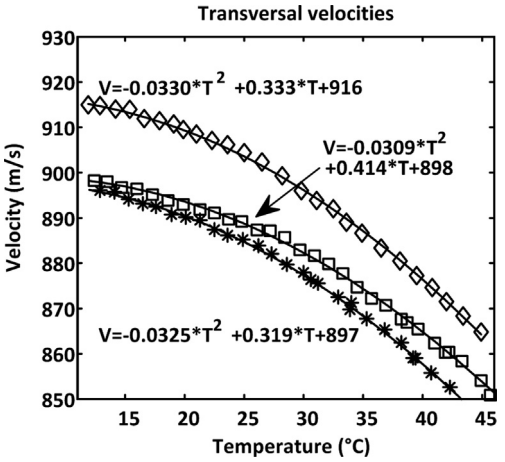

Fig. 6. Transversal velocity temperature dependency of sintered PA12 under various RH conditions (◆ RH 40%, □ RH 55%, • RH 80%).

fitted linearly. It presents no noticeable dependency on RH. Its temperature coefficient is $\gamma_T = -1.52$ m s^{-1} °C^{-1} with a shear velocity at the origin equals to $V_{T0} = 800$ m s^{-1}.

PA12 shows interesting features. As it can be seen in Fig. 6, its temperature behavior is best fitted by a quadratic polynomial, and RH conditions have a clear effect on the transversal velocity. Its temperature coefficients are $\gamma_T^2 = -0.0321$ m^2 s^{-2} °C^{-1} and $\gamma_T^1 = 0.355$ m s^{-1} °C^{-1}, but with offsets V_{T0} of 916 m s^{-1}, 898 m s^{-1} and 897 m s^{-1} corresponding, respectively, to 40% RH, 55% RH and 80% RH.

Again by comparison, thermal shear velocity coefficient for copper is linear and about twice as small as in ABS, close to -0.75 m s^{-1} °C^{-1} [12].

Table 1 gathers the standard deviations std and maximum errors to the interpolated curve associated with the measurements. Uncertainty is estimated using a quadratic model of data $\tilde{x}_i$ as in Equation (8).

$$\text{std} = \sqrt{\frac{1}{n}\sum_{i=1}^{n}(x_i - \tilde{x}_i)^2} \tag{8}$$

For the two sample materials, we observe a maximum standard deviation of ±1% for all velocities with a maximum of ±3.9% deviation to the quadratic models over the full temperature range.

PA12 is sensitive to humidity, especially for transversal waves. The effect of humidity on longitudinal waves is indeed less significant in these experiments which can be explained by the fact that PA12 is relatively porous. Therefore, water enters the material and, because transversal waves do not propagate in fluids, contrarily to longitudinal waves, they are more affected by humidity.

6. Damping effect

Damping is another strong effect that comes with temperature increase. Another experimental set-up was designed to obtain better measurements of amplitudes. Each sample of thickness 3 mm was mechanically coupled to transducers M110 and V153 with coupling agent

Table 1
Standard deviation and maximum error on velocity measurements relatively to the quadratic approximation for materials ABS and PA12 and for both type of fundamental waves, longitudinal (L) and transversal (T).

		40% RH		55% RH		80% RH	
		STD (%STD)	MAX (%MAX)	STD (%STD)	MAX (%MAX)	STD (%STD)	MAX (%MAX)
ABS	L	± 18 m s^{-1} ($\pm 0.87\%$)	± 78 m s^{-1} ($\pm 3.9\%$)	± 21 m s^{-1} ($\pm 1\%$)	± 66 m s^{-1} ($\pm 3.1\%$)	± 16 m s^{-1} ($\pm 0.79\%$)	± 62 m s^{-1} ($\pm 3.1\%$)
	T	± 1.3 m s^{-1} ($\pm 0.17\%$)	± 6.2 m s^{-1} ($\pm 0.8\%$)	± 0.82 m s^{-1} ($\pm 0.11\%$)	± 7 m s^{-1} ($\pm 0.91\%$)	± 1 m s^{-1} ($\pm 0.14\%$)	± 9.3 m s^{-1} ($\pm 1.3\%$)
PA12	L	± 5.9 m s^{-1} ($\pm 0.31\%$)	± 26 m s^{-1} ($\pm 1.5\%$)	± 4.5 m s^{-1} ($\pm 0.24\%$)	± 21 m s^{-1} ($\pm 1.1\%$)	± 5.4 m s^{-1} ($\pm 0.28\%$)	± 32 m s^{-1} ($\pm 1.8\%$)
	T	± 0.35 m s^{-1} ($\pm 0.039\%$)	± 1.7 m s^{-1} ($\pm 0.19\%$)	± 0.36 m s^{-1} ($\pm 0.041\%$)	± 2.2 m s^{-1} ($\pm 0.26\%$)	± 0.47 m s^{-1} ($\pm 0.054\%$)	± 1.7 m s^{-1} ($\pm 0.2\%$)

(Panametrics – SWC). Two echoes were recorded in a pulse-echo method in order to avoid differences in mounting conditions or temperature sensitivity of transducers. To avoid misalignment that may influence the measured amplitude, and thus the attenuation estimation, only one transducer is preferred. However, in the case of transversal waves, attenuation may be very important. As a consequence one transducer was used for estimating attenuation of longitudinal waves and two transducers were used for estimating attenuation of transversal waves. In that latter case, the travelling path is reduced so that the signal to noise ratio is improved. In order to limit the transducer misalignment, a special tool was designed. Slow temperature cycles are imposed to limit hysteresis and obtain stable amplitude measurements of the first two echoes. As described in the work of [13] and assuming a +1 reflection coefficient value at the air-plastic interface, attenuation is calculated taking into account both diffraction and dilatation effects:

$$\alpha(\mathrm{T}) = \frac{1}{2h^{*}\left[1 + C_{ThermExp}(\mathrm{T} - 25)\right]}\left[\ln\left(\frac{|S_1|\cdot|D_{3h}|}{|S_2|\cdot|D_h|}\right)\right], \qquad (9)$$

where α is the attenuation in Np m^{-1}, h is the thickness at 25 °C, $C_{ThermExp}$ is the correction factor due to thermal expansion, $|D_{h,3h}|$ are the modulus of diffraction correction terms for traveling distances and $S_{1,2}$ are the amplitudes of first and second echoes for 5 MHz or 1 MHz spectral component. Fig. 7 shows longitudinal attenuation in dB cm^{-1} with $\alpha_{sB} = 20\log_{10}(\alpha)$. Signals are noisy for both materials but with stable mean values. No sensitivity to RH conditions appears for PA12 whereas ABS exhibits more attenuation with RH. We obtain an attenuation of about 15.3 dB cm^{-1} for ABS and 27.1 dB cm^{-1} for PA12 at 25 °C. Above 25 °C, attenuation in PA12 tends to increase with temperature at a rate of 0.07 dB cm^{-1} °C^{-1} and the trend is decreasing for ABS. Longitudinal attenuations measured by Nishikawa [11] are in agreement with our measurements. Moreover, the peak shows a negative value of about −18 °C in Nishikawa's measurements which can explain the decreasing tendency observed in Fig. 7. In the work of [14], we find values of 11.3 dB cm^{-1} for injected grey ABS and 2.9 dB cm^{-1} for Nylon 6/6 at 25 °C and 5 MHz operating conditions. It should be noted that the work of Selfridge is carried out in the time domain with broad-band transducers and that attenuation in Nylon is related to a plain non-porous material, which is not the case of sintered thermoplastics.

Fig. 8 shows transversal attenuations in both materials at the same three RH conditions and in the 10 °C to 70 °C temperature range. The effect of humidity can clearly be observed. For ABS, it consists mainly in a translation of the attenuation coefficient, whereas PA12 exhibits a change of slope. Above 40 °C, the second echo is too weak to be measured, but the trend is in favor of an increase of the attenuation coefficient. In ABS, attenuation is unexpectedly

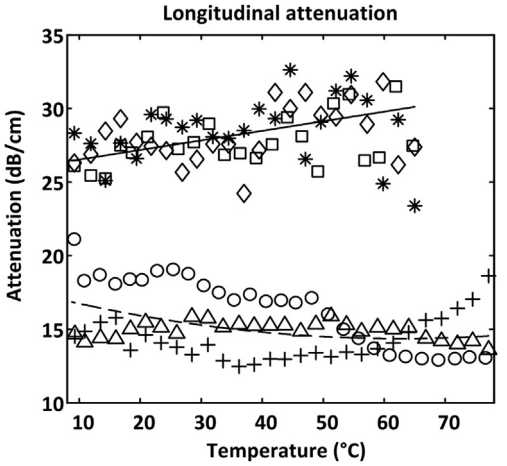

Fig. 7. Longitudinal attenuation in ABS (+ RH 40%, ○ RH 55%, Δ RH 80%) and PA12 (◆ RH 40%, □ RH 55%, * RH 80%) under various temperature and RH conditions and at 5 MHz operating frequency.

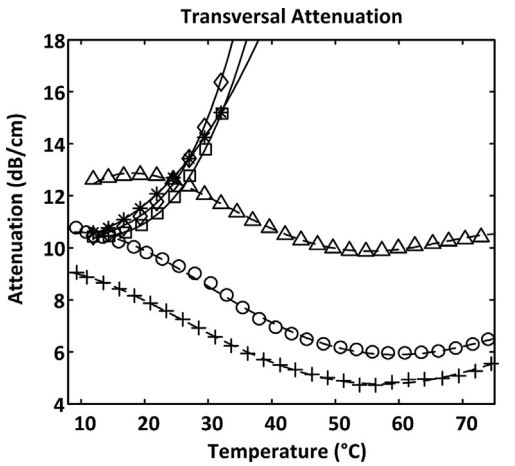

Fig. 8. Transversal attenuation in ABS (+ RH 40%, ○ RH 55%, Δ RH 80%) and PA12 (◆ RH 40%, □ RH 55%, * RH 80%) according to temperature and at 1 MHz operating frequency.

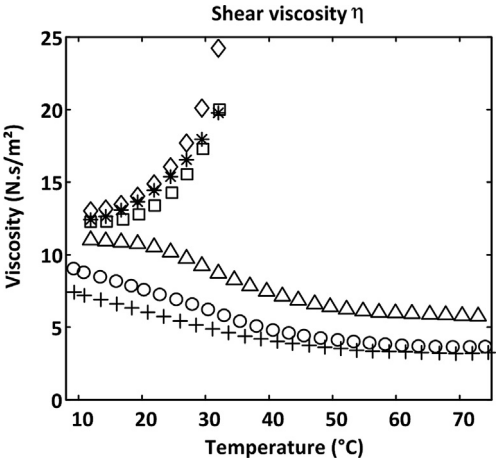

Fig. 9. Viscosity coefficient η in ABS (+ RH 40%, ○ RH 55%, Δ RH 80%) and PA12 (◆ RH 40%, □ RH 55%, * RH 80%) according to temperature.

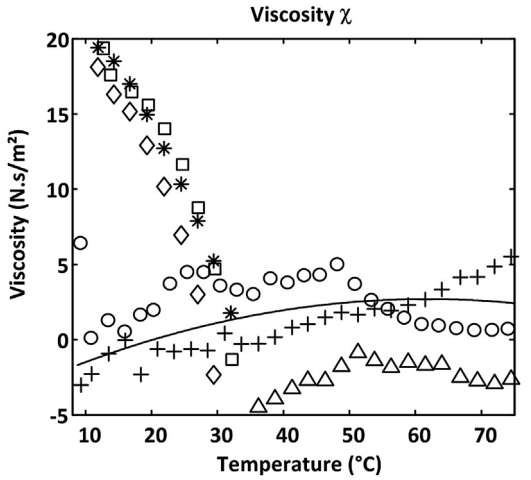

Fig. 11. Viscosity coefficient χ in ABS (+ RH 40%, ○ RH 55%, Δ RH 80%) and PA12 (◆ RH 40%, □ RH 55%, * RH 80%) according to temperature and at various RH conditions.

reduced when temperature is increased, to a maximum at about 55 °C.

In order to analyze these results, we recall that in a viscous medium the signal loss follows an exponential law of the form $s = S_0 \cdot e^{-\alpha z}$ [15], where α is the attenuation constant given by the following expression:

$$\alpha = \frac{\eta \omega^2}{2V^3 \rho}, \tag{10}$$

where, η is the viscous constant in N s m^{-2} for the considered material, ω the angular frequency, ρ the density and V the velocity. Following [16], the generalized Hooke's law with a Kelvin-Voigt model is expressed as:

$$T_{ij} = C_{ijkl} \cdot S_{kl} + \eta_{ijkl} \cdot \frac{dS_{kl}}{dt}, \tag{11}$$

where T_{ij}, is the stress tensor, S_{kl}, the strain tensor, C_{ijkl} the elastic stiffness tensor and η_{ijkl}, the viscous tensor. Using Eq.

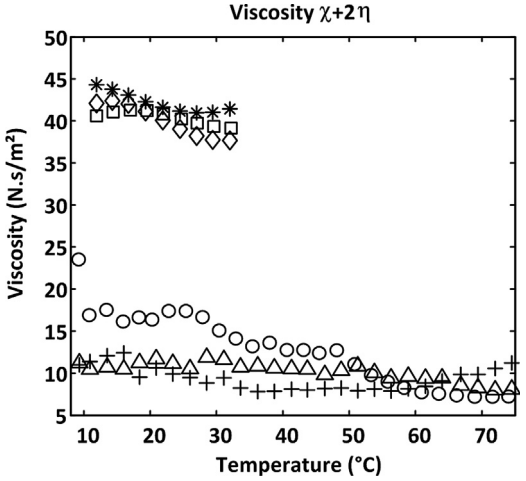

Fig. 10. Viscosity coefficient $\chi + 2\eta$ in ABS (+ RH 40%, ○ RH 55%, Δ RH 80%) and PA12 (◆ RH 40%, □ RH 55%, * RH 80%) at various temperature and RH conditions.

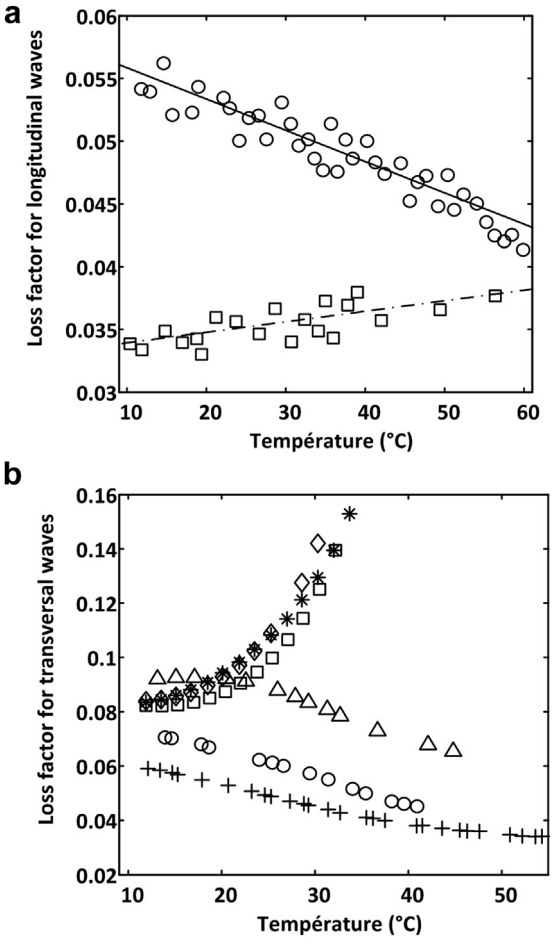

Fig. 12. Loss factors as function of temperature. (a) Loss factor of ABS (○) and PA12 (□) for longitudinal waves. Effect of moisture is negligible; (b) Loss factor of ABS (+ RH 40%, ○ RH 55%, Δ RH 80%) and PA12 (◆ RH 40%, □ RH 55%, * RH 80%) for transversal waves.

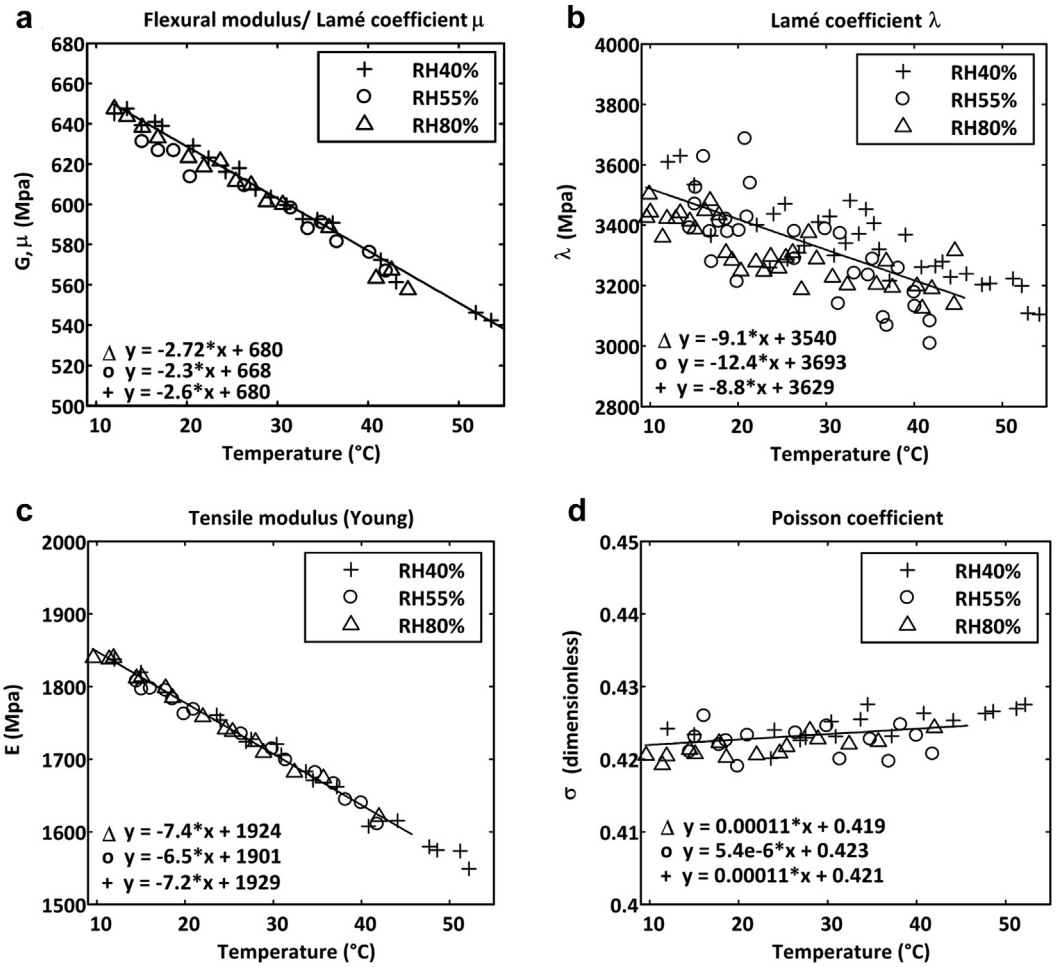

Fig. 13. Computed temperature dependency of physical parameters for ABS, derived from longitudinal and transversal wave velocities. (a) Flexural modulus or Lamé parameter μ; (b) Lamé parameter λ; (c) Young's modulus; (d) Poisson's ratio.

(11) in the expression of the propagation equation in the case of an isotropic solid, it is demonstrated in [17] that the attenuation constant relies on the fundamental wave mode. For the transversal and longitudinal modes, the attenuation constants are expressed, respectively, as:

$$\alpha_T = \frac{\eta\omega^2}{2V_T^3\rho} \text{ and } \alpha_L = \frac{(\chi+2\eta)\omega^2}{2V_L^3\rho}, \tag{12}$$

where η is the shear viscous coefficient and χ the compressibility viscous coefficient for an isotropic material, both are expressed in N s m^{-2}. ρ is the density, ω the angular frequency, and V_T and V_L the transversal and longitudinal wave velocities, respectively.

The T temperature dependency of the longitudinal or transversal velocities is reformulated for a linear model:

$$V = \gamma T + V_0 = V_0(1+\beta T) \text{ with parameter } \beta = \gamma/V_0 \tag{13}$$

We recall that the temperature coefficient for the PA12 longitudinal velocity is $\gamma_L = -5.31$ m s^{-1} °C^{-1} with $V_{L0} = 2126$ m s^{-1}. Consequently, we have $\beta = -0.0025$ °C^{-1} for the normalized temperature coefficient. The same treatment applied to ABS yields $\beta = -0.00125$ °C^{-1}.

Transversal velocity approximation yields for ABS a linear coefficient $\beta = -0.002$ °C^{-1} and for PA12, two quadratic coefficients for the three RH conditions.

Considering the small values taken by β, a first order development for the temperature linearly dependent velocity raised to a power of three yields:

$$V^3 = V_0^3(1+\beta T)^3 \approx V_0^3(1+3\beta T) \tag{14}$$

and in the case of a quadratic approximation, we get:

$$V^3 = V_0^3\left(1+\beta_1 T+\beta_2 T^2\right)^3 \approx V_0^3\left(1+3\beta_1 T+3\left(\beta_2+\beta_1^2\right)T^2\right) \tag{15}$$

The transversal attenuation coefficient can then be reformulated with the previous approximations and density taken at 25 °C.

$$\alpha_T \approx \frac{\eta\omega^2}{2V_{T0}^3\rho_0}\left(1-3\beta_1 T-3\left(\beta_2+\beta_1^2\right)T^2\right)\left(1+3C_{ThermExp}(T-23)\right) \tag{16}$$

Based on the same principle, the longitudinal coefficient can be expressed as:

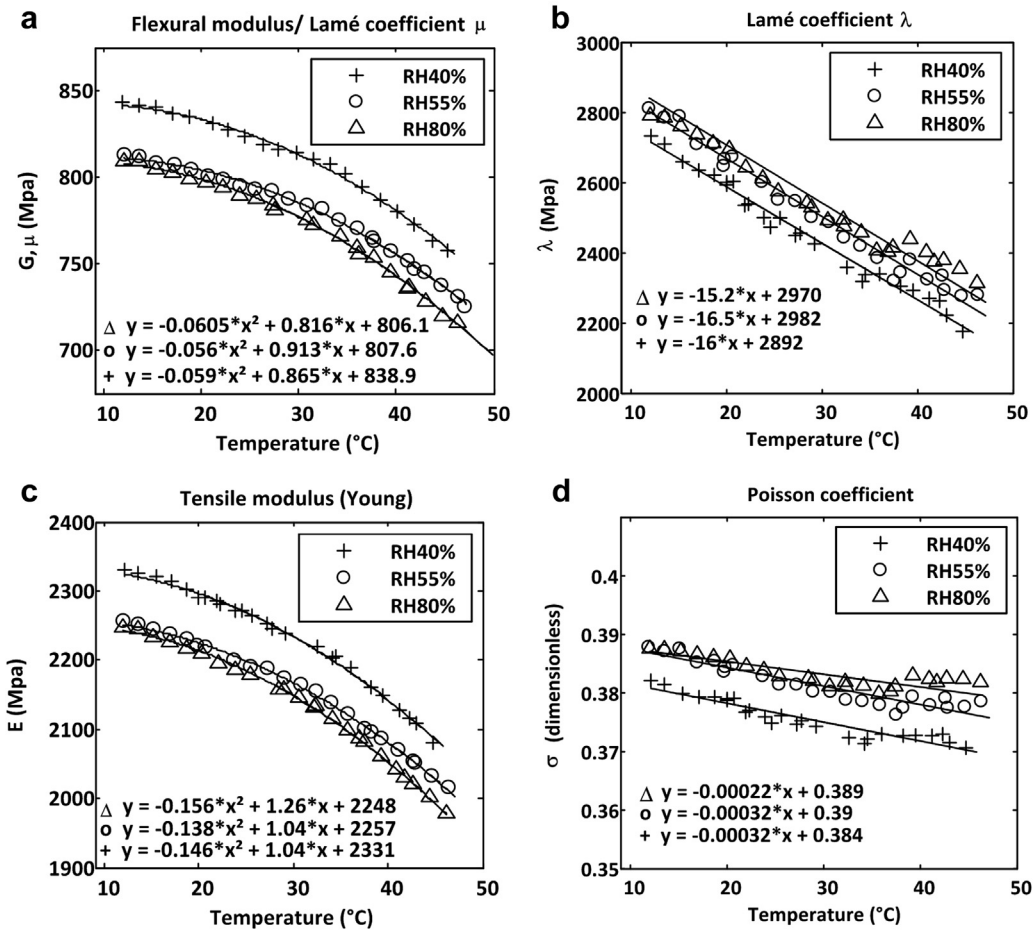

Fig. 14. Computed temperature dependency of physical parameters for PA12, derived from longitudinal and transversal wave velocities. (a) Flexural modulus or Lamé parameter μ; (b) Lamé parameter λ; (c) Young's modulus; (d) Poisson's ratio.

$$\alpha_T \approx \frac{(\chi + 2\eta)\omega^2}{2V_{L0}^3\rho_0}(1 - 3\beta_1 T)\left(1 + 3C_{ThermExp}(T - 23)\right) \qquad (17)$$

Considering only the experimental values taken by β_1 for the longitudinal wave velocity temperature dependency in ABS and PA12, we can expect from Eq. (17) a longitudinal attenuation increase of at least 24% in ABS and 49% in PA12 for the whole temperature range. The mean curves in Fig. 7 shows the corresponding trends with a slope that is larger for PA12 than for ABS.

Based on the measurement of shear and longitudinal attenuations in both materials, we can now evaluate the viscous parameters for ABS and PA12. The shear viscosity parameter η presents the same dependency to RH conditions as the transversal attenuations α_T (see Fig. 9). As expected from Eq. (16), parameter η shows quadratic dependency on velocity.

Fig. 10 shows the dilatational viscosity $(\chi + 2\eta)$ based on the longitudinal attenuation models. In ABS, dilatational viscosity tends to decrease with temperature until a minimum of 6.8 N s m^{-2} and with small differences of slope with temperature.

Fig. 11 shows the compressibility viscous coefficient χ, deduced from the shear viscosity η and dilatational viscosity $\chi + 2\eta$. Because dilatational viscosity was almost linear, compressibility viscosity reflects the opposite trend to shear viscosity and exhibits quadratic curves. Values below zero suggest undervalued longitudinal attenuation for 80% RH in ABS. The compressional viscosity follows a quadratic increase in ABS and reaches a maximum mean value of 2.3 N s m^{-2}. In PA12, we observed the opposite trend as regards shear viscosity. Although PA12 compressibility viscosity falls to zero at 35 °C, the value must stay positive and reaches a minimum flat tendency

Table 2
Mechanical parameter values for ABS and sintered PA12 retrieved from manufacturer datasheets [7,8] (evaluated from measurements).

	Lamé μ	Lamé λ	Young's modulus	Poisson's ratio
ABS@25°C	656 MPa (611 MPa)	3442 MPa (3383 MPa)	1862 MPa (1738.4 MPa)	0.42 (0.423)
PA12@25°C	1285 MPa (795.4 MPa)	1835 MPa (2569.3 MPa)	1600 MPa (2271 MPa)	0.38 (0.382)

for higher temperatures. In consequence, we assume shear viscosity in PA12 to evolve with a flat tendency above 35 °C to keep dilatational viscosity linear.

Finally the most important result in this section is the fact that transversal attenuation is sensitive to RH and tends to decrease for ABS, whereas it strongly increases for PA12. This result can be related to the material manufacturing processes, which lead to intrinsic structural differences in the two materials.

In other work [18,19], damping behavior of a material if often expressed as the loss factor:

$$\eta_{L,T} = \frac{\alpha_{L,T} V_{L,T}}{\pi f}, \tag{18}$$

where the attenuation α and the velocity V are considered for longitudinal or transversal waves. Without results, the loss factors are shown in Fig. 12 for the both materials. Effect of humidity is negligible in the case of longitudinal waves.

7. Physical properties of ABS and PA12

Knowing the longitudinal and transversal wave velocity temperature dependencies, it is now possible to evaluate some other temperature dependent physical parameters. Fundamental waves velocities are related to coefficients c_{11}, c_{12} and c_{44} of elastic stiffness tensor and thus to Lamé parameters (μ, λ), Young's modulus E and Poisson's ratio σ as shown in Eq. (19) [16,20].

$$\begin{cases} V_L = \sqrt{\dfrac{c_{11}}{\rho}} = \sqrt{\dfrac{\lambda + 2\mu}{\rho}} \\ V_T = \sqrt{\dfrac{c_{11} - c_{12}}{2\rho}} = \sqrt{\dfrac{\mu}{\rho}} \end{cases} => \begin{cases} \mu = V_T^2 \cdot \rho \\ \lambda = \rho \cdot \left(V_L^2 - 2 \cdot V_T^2\right) \\ E = \mu \cdot \dfrac{3 \cdot \lambda + 2 \cdot \mu}{\lambda + \mu} = \rho \cdot V_T^2 \cdot \dfrac{3 \cdot V_L^2 - 4 \cdot V_T^2}{V_L^2 - V_T^2} \\ \sigma = \dfrac{\lambda}{2 \cdot (\lambda + \mu)} = \dfrac{V_L^2 - 2 \cdot V_T^2}{2 \cdot \left(V_L^2 - V_T^2\right)} \end{cases} \tag{19}$$

Fig. 13 shows derived mechanical properties for ABS. For this material, velocities decrease linearly with temperature and are not influenced by RH. Consequently, all physical parameters are linearly temperature dependent.

Fig. 14 shows the same results for sintered PA12. The quadratic evolution of the fundamental waves according to temperature leads to the same quadratic behavior of the mechanical parameters. Furthermore, sensitivity of shear waves to RH introduces some dispersion between the physical parameters.

Clear quadratic evolution of the transversal waves is reflected on the Lamé coefficient μ (or flexural modulus) or Young's tensile modulus.

These results can be compared to other values given by manufacturers and found in Table 2 at 25 °C. Noticeable differences can be observed. We believe this can be explained by several factors such as: grain composition, manufacturing process and ageing. Goodridge et al. [21] have observed increase of Young's Modulus which is in agreement with our values after some weeks of ageing for laser sintered PA12 samples.

8. Conclusions

This paper presents a comparative study of two types of plastic both eligible as potential ultrasonic touch interfaces either in the perspective of fast prototyping evaluation or as end-user final products. Selective laser sintering of a PA12 plastic powder is convenient for fast prototyping but exhibits stronger sensitivity towards temperature and RH conditions than injected ABS. Simultaneously, fundamental wave velocity decay with temperature involves strong viscous damping for 58 μm mean grain size sintered PA12, whereas it remains stable for ABS. This affects signal transmission in these materials and, subsequently, should be considered in the design guidelines of touch interfaces.

Thermal velocity coefficient is linear for longitudinal waves in both materials. This behavior is also linear for transversal waves in ABS. However, sintered PA12 exhibits unusual quadratic evolution for this fundamental wave [11,12,22]. Moreover, ABS is not sensitive to humidity whereas transversal waves in PA12 present offset along the different humidity conditions. These observations are possibly the signature of internal granular structure of sintered plastics which could lead to accumulation of water in sintered plastic structure. A quantitative study of drying rate would be fruitfully investigated. It is also of particular importance knowing the operating principle of ultrasonic touch interfaces, which are based on the generation and detection of plate bending waves, which rely on the thermal velocity coefficients of fundamental waves. Future work will present temperature dependency of guided Lamb waves and how it affects the stability of the touch recognition algorithm.

References

[1] Y. Liu, J.-P. Nikolovski, N. Mechbal, M. Hafez, M. Verge, Tactile objects based on an amplitude disturbed diffraction pattern method, Applied Physics Letters vol. 95 (2009), p. 251904.
[2] R.-K. Ing, D. Cassereau, M. Fink, J.-P. Nikolovski, Tactile touch plate with variable boundary conditions, Journal of the Acoustical Society of America vol.123 (2008), p. 3643.

[3] Y. Liu, J.-P. Nikolovski, N. Mechbal, M. Hafez, M. Vergé, An acoustic multi-touch sensing method using amplitude disturbed ultrasonic wave diffraction patterns, Sensors and Actuators A: Physical vol. 162 (2010), pp. 394–399.
[4] J.P. Nikolovski, Moderately reverberant learning ultrasonic pinch panel, IEEE Transactions on Ultrasonics, Ferroelectrics, and Frequency Control vol. 60 (2013).
[5] G. Ribay, S. Catheline, D. Clorennec, R.K. Ing, N. Quieffin, M. Fink, Acoustic impact localization in plates: properties and stability to temperature variation, IEEE Transactions on Ultrasonics, Ferroelectrics, and Frequency Control vol. 54 (2007), pp. 378–385.
[6] Y. Lu, J.E. Michaels, A methodology for structural health monitoring with diffuse ultrasonic waves in the presence of temperature variations, Ultrasonics vol. 43 (2005), pp. 717–731.
[7] Ensinger, http://www.ensinger-inc.com/products.cfm?page=product&product=tecaran+abs, visited, 2014.
[8] DuraForm ®PA Plastic, http://www.3dsystems.com/materials/duraformr-pa, visited, 2014.
[9] A.B. Temsamani, S. Vandenplas, M.L. Lumöri, L. Van Biesen, Experimental validation for the diffraction effect in the ultrasonic field of piston transducers and its influence on absorption and dispersion measurements, IEEE Transactions on Ultrasonics, Ferroelectrics, and Frequency Control vol. 48 (2001).
[10] P.H. Rogers, A.L. Van Buren, An exact expression for the Lommel-diffraction correction integral, Journal of the Acoustical Society of America vol. 55 (1974), p. 724.
[11] K. Nishikawa, Y. Hirose, O. Urakawa, K. Adachi, A. Hatano, Y. Aoki, Ultrasonic absorption and relaxations in ABS composite polymers, Polymer vol. 43 (2002), pp. 1483–1490.
[12] K. Salama, C.K. Ling, The effect of stress on the temperature dependence of ultrasonic velocity, Journal of Applied Physics vol. 51 (1980), p. 1505.
[13] M. Treiber, J.-Y. Kim, L.J. Jacobs, J. Qu, Correction for partial reflection in ultrasonic attenuation measurements using contact transducers, Journal of the Acoustical Society of America vol. 125 (2009), pp. 2946–2943.
[14] A.R. Selfridge, Approximate material properties in isotropic materials, IEEE Transactions on Sonics and Ultrasonics vol. 32 (1985), pp. 381–394.
[15] G.S. Kino, Acoustic Waves: Devices, Imaging, and Analog Signal Processing, in: Prentice-Hall Signal Processing Series, Prentice Hall, 1987.
[16] J.L. Rose, Ultrasonic Waves in Solid Media, Cambridge, 2004.
[17] D. Royer, E. Dieulesaint, Elastic Waves in Solids 1, Springer-Verlag Berlin and Heidelberg GmbH & Co. K, 2000.
[18] U.B. Buchholz, M. Jaunich, W. Stark, W. Habel, B.A.T. Petersson, Acoustic data of cross linked polyethylene (XLPE) and cured liquid silicone rubber (LSR) by means of ultrasonic and low frequency DMTA, IEEE Transactions on Dielectrics and Electrical Insulation vol. 19 (2012), pp. 558–566.
[19] L. Cremer, M. Heckl, B.A.T. Petersson, Structure-borne Sound – Structural Vibrations and Sound Radiation at Audio Frequencies, third ed., Springer, 2005.
[20] D.K. Pandey, S. Pandey, Ultrasonics: a technique of material characterization, in: D. Dissanayake (Ed.), Acoustic Waves, 2010, pp. 397–430.
[21] R.D. Goodridge, R.J.M. Hague, C.J. Tuck, Effect of long-term ageing on the tensile properties of a polyamide 12 laser sintering material, Polymer Testing vol. 29 (2010), pp. 483–493.
[22] V. Rajendran, N. Palanivelu, B.K. Chaudhuri, A device for the measurement of ultrasonic velocity and attenuation in solid materials under different thermal conditions, Measurement vol. 38 (2005), pp. 248–256.